Pure Appl. Chem., Vol. 84, No. 12, pp. 2653–2675, 2012.
http://dx.doi.org/10.1351/PAC-CON-11-11-05

Interface engineering: Boosting the energy conversion efficiencies for nanostructured solar cells*

Guodong Liu, Shulin Ji, Guoping Xu, and Changhui Ye‡

Anhui Key Laboratory of Nanomaterials and Technology and Key Laboratory of Materials Physics, Institute of Solid State Physics, Chinese Academy of Sciences, Hefei 230031, China

Abstract: Nanostructured solar cells have attracted increasing attention in recent years because their low cost and ease of preparation offer unique advantages and opportunities unavailable with conventional single-crystalline solar cells. The efficiencies of this kind of solar cell largely depend on the interfacial structure owing to the large specific interface areas and the inherent high density of interface states. In this review article, strategies of interface engineering will be introduced in detail. The up-to-date progress and understanding of interface engineering and its role in influencing the efficiency of nanostructured solar cells will be discussed. Some of the representative examples of the interface engineering method will be presented wherever necessary. Continued boosting of the energy conversion efficiency for nanostructured solar cells is anticipated in the coming years and will bring this kind of solar cell to the status of commercialization.

Keywords: interfaces; interface engineering; nanostructured materials; nanostructured solar cells; quantum dots; solar energy.

INTRODUCTION

Photovoltaic (PV) technologies are attracting increasing attention as the need for renewable energy sources to replace unsustainable energy technologies becomes more urgent. Integration of nanostructured materials in PV devices has been demonstrated to open the possibilities to develop low-cost solar cells [1,2]. In fact, a number of new PV technologies are emerging, among these, nanostructured solar cells, including quantum dot-sensitized solar cells (QDSCs) [3,4], extremely thin absorber layer solar cells [5,6], nanocrystal Schottky solar cells [7], and quantum dot-depleted heterojunction solar cells [8,9], have received more and more attention owing to the outstanding advantages of quantum dots (QDs) [10], such as the high extinction coefficient [11], size and compositional dependent absorption [11,12], and large intrinsic dipole moment [13,14]. Narrow bandgap sulfide semiconductors, such as PbS [15,16], CdS [17–20], CdSe [21,22], and Sb_2S_3 [23,24], are promising candidates as sensitizers for wide bandgap semiconductors (e.g., TiO_2, ZnO, and SnO_2). Importantly, the synthesis of semiconductor QDs or QD layers with solution-based approaches, such as molecular linker-mediated self-assembly [25], in situ chemical bath deposition (CBD) [6,24,26], electrodeposition from ionic liquids [27], and physisorption of QDs to the metal oxide substrate [28,29], take place at significantly lower tem-

Pure Appl. Chem.* **84, 2499–2675 (2012). A collection of invited papers based on presentations at the 7th International Conference on Novel Materials and their Synthesis (NMS-VII) and the 21st International Symposium on Fine Chemistry and Functional Polymers (FCFP-XXI), Shanghai, China, 16–21 October 2011.
‡Corresponding author

peratures than vapor-phase methods. The possibility of exploiting multiple exciton generation to obtain high efficiencies adds another potential advantage [30,31], therefore, an increasing number of research groups have been drawn toward studying and realizing nanostructured solar cells.

These kinds of solar cells are conceptually similar to dye-sensitized solar cells (DSCs) [32]. For example, they are based on a mesoporous structure of a wide bandgap semiconductor, typically TiO_2 or ZnO (except for nanocrystal Schottky solar cells that do not necessarily involve the wide bandgap semiconductor), sensitized by a light-harvesting material with a narrow bandgap, permeated with a redox electrolyte, and sandwiched by a counter electrode. For QDSCs, a light-absorbing semiconductor was deposited on the internal surface of a porous transparent oxide taking the place of a dye, and a polysulfide electrolyte was widely used as a hole-extraction medium [33–37] instead of the polyiodide electrolyte I^-/I^{3-} redox couple used in DSCs, because many metal sulfides are not chemically compatible with I^-/I^{3-} redox couple [3,38]. Solid hole conductor CuSCN [6,39] was usually used in solid QDSCs. Provided that the energy level alignment [40] is suitable for carrier transport, the photogenerated carriers can inject into the adjacent electron and hole conducting media, i.e., electrons into TiO_2 and holes into the electrolyte. Nevertheless, in a real QDSC, transport, recombination, and transfer processes for photogenerated electrons and holes in QDs are rather complicated [3,41]. Bisquert's group [41] has summarized the possible processes of photogenerated carriers in QDSCs as shown in Fig. 1, where the photogenerated electrons can inject into TiO_2 (I1) and transport in it (T1), or can be trapped by the gap states in TiO_2 (I2) or in QD (Tr1), or can directly recombine with photogenerated holes (R1) in QDs, depending on the band energy alignment. In the transport process through TiO_2 electrons can be trapped in this material (Tr3), and subsequently be released to the conduction band (CB) or back-injected into the semiconductor QDs (I3). For QDSCs, a large fraction of the wide bandgap semiconductor surface might be in direct contact with the hole conductor, hence the trapped electrons may be lost to recombination with holes in the hole-transporting medium (R4), besides the recombination with trapped holes by gap states (R2, 3). Simultaneously, the photogenerated holes undergo similar processes to electrons. For efficient solar cell operation, charge-transfer and -transport processes are required to be faster than recombination, and processes I1, I4, I5, T1, and T2 are desired [3].

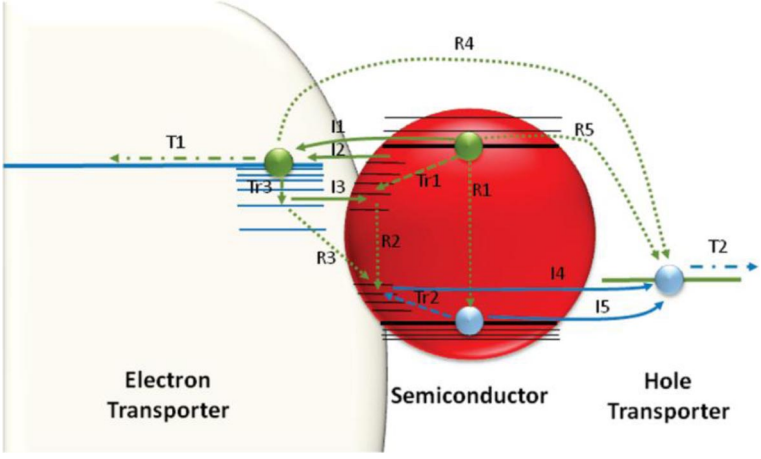

Fig. 1 (Color online) Charge-transfer and -transport processes for photogenerated electrons (green arrows) and holes (blue arrow) in QSSC. A semiconductor QD with discrete energy levels is taken as an example. For clarity requirements, each arrow could denote more than one process. Injection (solid arrow), trapping (dashed arrow), recombination (dotted arrow), and transport (dash-dot arrow) are indicated. (Reprinted with permission from ref. [41]; copyright © 2010, American Chemical Society.)

It is widely accepted that there is generally a large density of surface states or trapping sites at the surface of nanostructured materials [42–44] and at the interface between QDs and wide bandgap semiconductors [45]. For a solar cell device composed of various working elements, we use interface throughout the rest of this work. The relevance of interface states stems from the fact that they can dominate charge-transport kinetics across the junction of different materials and act as traps or recombination centers for carriers. Although nanostructured solar cells are progressing rather rapidly, the efficiency is limited to ~5 % [46,47], still lagging behind DSCs [34] and organic solar cells. One of the important reasons is that the higher recombination rate of photogenerated charge carriers at the interface of QDs and wide bandgap semiconductors [3] and possible huge leaking currents, inherent in the case of nanostructured materials with large specific surface area [41,48,49]. Nevertheless, in the past few years, an encouraging improvement in the overall performance of nanostructured solar cells has been attained by means of new routes of sensitization (such as attaching presynthesized colloidal QDs to the electrode material with a bifunctional linker molecule [15,25,36,50–54], direct growth of the QDs on the electrode surface by chemical reaction of ionic species [49,55–57], and QDs co-sensitization [58]), optimized counter electrodes [16] and polysulfide electrolyte [26,59], introduction of an energy barrier layer between QDs and wide bandgap semiconductors [17,22,60,61], and photoanode post-treatments (such as ZnS [21,62], amorphous TiO_2 [18,63,64] or SiO_2 [22] treatments, dipole adsorption [19,58,65], ion insertion [46,49,66], modification with $ZnCl_2$ [67,68] or $CdCl_2$ [69]). Until now, much work has indicated that surface treatment or post-treatment is one of the most successful methods to control the electron injection and recombination processes, adjust the band alignment, and increase the efficiency and stability of the solar cells [3,18,19,21,23,46,48,49,62,70]. These treatments can be employed to protect QDs [21,54,62], passivate wide bandgap semiconductors [17,64], and modify the metal electrode [16,71]. Surface modification via different approaches has been demonstrated to be a powerful tool to boost the energy conversion efficiencies of the devices. In this paper, we shall provide an overview of some common treatments employed at the cathode and anode interface of nanostructured solar cells. To be specific, we will mainly talk about QDSCs, however, these treatments are also applicable to other nanostructured solar cells.

INTERFACE ENGINEERING

Interface engineering proves to be feasible for boosting the performance of nanostructured solar cells. In this section, we first discuss the approaches to controlling the attachment of QDs to the wide bandgap semiconductors, and then introduce the concept of interface passivation, and finally deal with the idea of band structure modification of the interface between the QDs and the anode.

There are three main methods of QD adsorption on wide bandgap semiconductors: (i) deposition of presynthesized colloidal QDs by linker-assisted adsorption (LA), (ii) deposition of presynthesized colloidal QDs by direct adsorption (DA), and (iii) in situ growth of QDs by CBD. The first method using a molecular linker allows a control of the size and shape of the QDs by the colloidal synthesis, which is not possible with the direct growth of QDs on the semiconductor surface [72]. Additionally, the introduced linker could affect the interfacial charge-transfer dynamics from QDs to wide bandgap semiconductors [73,74] and thus the device performance [15,54]. Referred to the direct growth of QDs on the semiconductor surface, many groups focused on the interface between QD-sensitized electrodes and electrolyte to reduce the recombination of electrons in wide bandgap semiconductor with electrolyte. Additionally, some studies using a combination of both linked colloidal QDs and CBD have been carried out [70,75]. It has been proved that in QDSCs, the recombination of electrons in TiO_2 with electrolyte was the most important process detrimental to PV cell efficiencies. Here we summarize the role the molecular linkers played in photocarrier transport, and then discuss the treatment for the interface between QD-sensitized electrodes and the electrolyte.

Molecular linkers passivated on the QD/TiO_2 interface

Owing to the structure differences between the dye and the QDs, one of the challenges is the optimization of the QD/TiO_2 interface for efficient QD → TiO_2 electron injection. It has been shown that both thiols [76] and amines [77] bind strongly to the surface of sulfide particles. Carboxyl groups, on the other hand, do not adsorb well to the CdS surface [50]. The widely used linkers are the bifunctional thiophenol derivants that diminish the coagulation of the colloidal QDs and ensure monolayer surface coverage, without changing the absorption spectra relative to those of QDs alone [25]. The linker type and/or length could obviously influence the performance of this kind of solar cell [36,54].

Many groups [73,74,78–82] have focused on the electron injection and interfacial charge recombination in QDSCs by changing the length/type of the linkers or the size/shape of the QDs to optimize charge-transport processes. Rachel and David [73,74] have characterized electron injection from photoexcited CdS QDs to TiO_2 nanoparticles as a function of the length and structure of mercaptoalkanoic acid (MAA) linker by steady-state emission quenching, nanosecond time-resolved emission, and nanosecond transient absorption. They pointed out that the multiple time scale electron injection yield increased with decreasing the chain length of MAA, which was consistent with the conclusion obtained by Hyun [15], and the multiexponential injection kinetics was caused by the electron transfer from a range of conduction-band and trap states. Meanwhile, the holes in relatively shallow (low-energy) trap states were reduced by linkers that effectively bridged QDs with TiO_2 [50], especially those linkers with aromatic groups [81,82], while the interfacial charge recombination dynamics on the microsecond time scale were independent of the chain length of MAA [73].

Many groups [25,51–53,72] have successfully achieved CdS or CdSe-sensitized TiO_2 PV cells with observable IPCE (incident photon-to-current efficiency) using thiophenol derivants as linkers. Kamat's group [25] has compared the IPCE of CdSe QD-sensitized TiO_2 QDSCs with three linker molecules of varying chain length, mercaptopro-pionic acid (MPA), thiolacetic acid (TAA), and mercapto-hexa-decanoic acid (MDA). As shown in Fig. 2, the CdSe/TiO_2 films using MPA and MDA as linker molecules showed the highest IPCE value of 12 % in these three films, and MPA was a little better than MDA. The key factor was that MPA and MDA as linkers can effectively bridge QDs and TiO_2, but TAA cannot, therefore, electron injection from photoexcited QDs to TiO_2 using MPA and MDA as linkers was much better than using TAA as a linker, given that the light-harvesting efficiency and charge collection efficiency were the same in these three films. Notably, this IPCE value was much lower than that

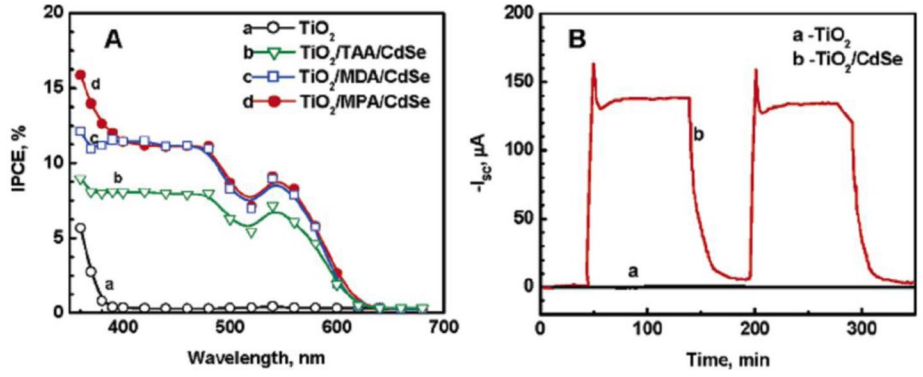

Fig. 2 (Color online) (A) Photocurrent action spectra of TiO_2 (a), and OTE/TiO_2/L/CdSe films where L (b) TAA, (c) MDA, and (d) MPA. Electrolyte 0.1 M Na_2S and Pt counter electrode. (B) Photocurrent vs. time profiles of (a) OTE/TiO_2 and (b) OTE/TiO_2/CdSe films using MPA as a linker molecule (0.2 M Na_2S electrolyte and illumination intensity 120 mW/cm^2). (Reprinted with permission from ref. [25]; copyright © 2006, American Chemical Society.)

of DSCs, indicating charge recombination or other loss mechanisms were major limiting factors in these QDSCs using molecular linkers passivated on the QD/TiO_2 interface.

The photoelectric conversion efficiency is also dependent on the linker structures. Recently, Bisquert's group [36] has studied the effect of linker structures on the performance of QDSCs. The structures of the three linkers were shown in Fig. 3 [36], MPA and TGA have a similar structure except that the chain length is longer for MPA, whereas cysteine has an additional amino group than MPA and TGA. The IPCE spectra for solar cells of CdSe QDs linked with these three molecules to the surface of TiO_2 were shown in Fig. 4 [36], where the efficiency for the cysteine case was the highest among the three cases (about five to six times that of the MPA case and about twice that of the TGA case). The authors [36] summarized the innate advantages of cysteine, which is not possible for MPA and TGA: (1) Cysteine adsorbed on TiO_2 surface can trap an electron or a hole, forming a cysteine radical, demonstrating the good stabilization of charges in this molecule [83]; (2) cysteine could anchor to the QDs via both the thiol and the amino groups. In such a way, the distance between the oxide particle and the QD would slightly decrease; (3) cysteine as an amino acid can be present as a zwitterionic structure, giving rise to a linker molecule with a strong dipole close to the QDs, which may create locally a strong stabilization of the charge-separated states.

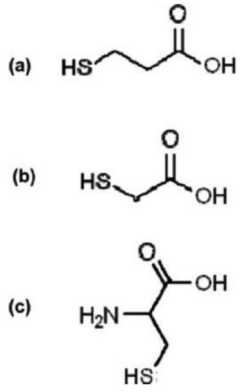

Fig. 3 The molecular structure of (a) MPA, (b) TGA, and (c) cysteine. (Reprinted with permission from ref. [36]; copyright © 2008, Institute of Physics.)

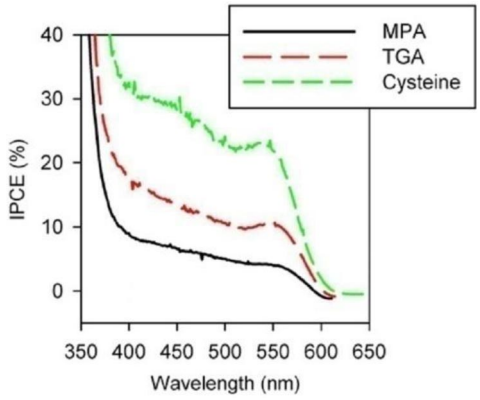

Fig. 4 (Color online) IPCE measured in the closed cell configuration (two-electrode system) with three different linker molecules (MPA, TGA, and cysteine) using the same QDs as sensitizers (2.8 nm). (Reprinted with permission from ref. [36]; copyright © 2008, Institute of Physics.)

Not only the electron injection can be modified by proper linkers but also a better energy level alignment can be realized by varying QDs size via linkers [72,80]. Kamat's group has conducted a systematic study for modulating the photoresponse of QDSCs by varying the size of CdSe QDs [80]. The QDs size can be determined by their first absorption peak positions [11] or by transmission electron microscopy (TEM) measurements. Considering the quantum confinement effect, the bandgap width will increase with decreasing particle size. Because of the small electron effective mass (m_e = 0.13 m_o) vs. the significantly larger hole mass (m_h = 1.14 m_o), most of the increase in the bandgap width was seen as a shift in the CB to more negative potentials (vs. NHE) [84]. This shift is expected to be favorable for injecting electrons from CdSe QDs into TiO_2. Figure 5a illustrates the principle of electron transfer from quantized CdSe into TiO_2, and Fig. 5b shows the electron injection rate on the energy difference between the CB energies of CdSe and TiO_2 ($-\Delta G$) [80]. As the particle size decreased from 7.5 to 2.4 nm, the electron injection rate was boosted by nearly 3 orders of magnitude.

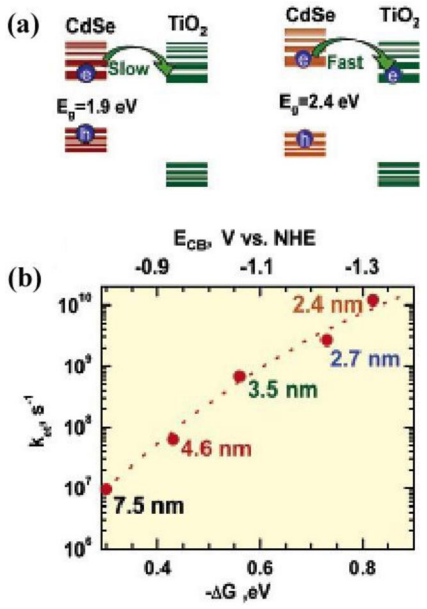

Fig. 5 (Color online) (a) Scheme illustrating the principle of electron transfer from quantized CdSe into TiO_2 and (b) the dependence of electron transfer rate constant on the energy difference between the CBs. Top axis represents assumed CdSe CB energy positions. (Reprinted with permission from ref. [80]; copyright © 2007, American Chemical Society.)

Considering that the IPCE is closely related with electron injection efficiency, the photoelectric conversion efficiency of QDSCs is supposed to be dependent on QDs size. Figure 6 presented the IPCE action spectra for different sized CdSe-sensitized TiO_2 nanoparticles (panel 6a) or nanotubes (panel 6b) [72], where the observed response peaks at 580, 540, 520, and 505 nm closely matched the absorption spectra (not shown), and the dependence of IPCE on particle size was stronger than that of absorption. The improved IPCE with smaller-sized QDs was proposed to arise from the enhanced rate of electron transfer from QDs to TiO_2 matrix [72].

The studies outlined above have revealed that surface-mediated self-assembly is an effective strategy for the assembly of QDs on the TiO_2 surface. This method affords precise control over the assembly process of materials, allowing for fundamental studies of the influence of interparticle distance [73,74] and linker structures [36] on the energy conversion efficiency of this kind of solar cell. However,

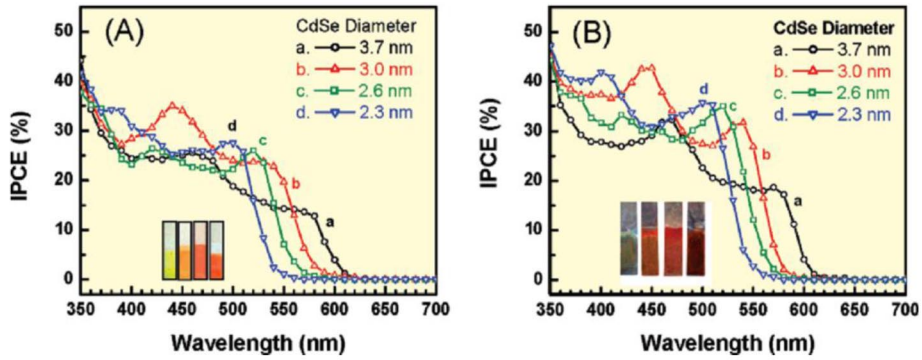

Fig. 6 (Color online) Photocurrent action spectra recorded in terms of IPCE of (A) OTE/TiO_2(NP)/CdSe and (B) Ti/TiO_2(NT)/CdSe electrodes. The individual IPCE responses correspond to (a) 3.7, (b) 3.0, (c) 2.6, and (d) 2.3 nm diameter CdSe QDs anchored on nanostructured TiO_2 films. (Reprinted with permission from ref. [72]; copyright © 2008, American Chemical Society.)

to date, the use of presynthesized colloidal QDs linked on the TiO_2 surface has led to less efficient solar cell devices compared with that of directly grown QDs. One possible explanation is that indirectly adsorbed colloidal QDs provide a low surface coverage [75], leading to inefficient light harvesting. On the other hand, Kamat's group [85] has obtained the newest results that there was no correlation between the measured electron-transfer rates and the performance of CdSe-sensitized solar cells, suggesting that other detrimental factors, such as charge recombination between photoinjected electrons and redox couples in the electrolyte [3,22], may be more vital than the electron injection process in limiting the efficiency of QDSCs [3,85]. Nevertheless, direct absorption can provide adequate QD loading (as opposed to linker-assisted) while maintaining the monodisperse layer of QDs and preventing their agglomeration on TiO_2 particles. Many researchers have focused on the DA of QDs on the TiO_2 and applied some interface control methods to improve the solar cell performance. The following section is focused on the procedure for effectively reducing the process of electron scavenging from the metal oxide by electrolyte and trap states.

Introducing an energy barrier layer

Several interfacial modifications of the sensitization of nanostructured solar cells with inorganic semiconductors and QDs have been recently studied. Gary [86] concluded that the surface states needed to be passivated and the recombination in the absorber layer reduced. Further, Bisquert's group [87] has demonstrated that charge recombination between electrons in TiO_2 and redox couples in the electrolyte was the main mechanism for degrading the performance of QDSCs. More scientists have put forward some constructive strategies [3,17–19,21,22,46,48,49,60–65,68,70,88–90] to reduce or suppress the recombination and other harmful charge-transport processes. In practice, a complete monolayer of QDs covered on the TiO_2 surface actually prevented the direct contact of TiO_2 matrix with the electrolyte, and further suppressed the recombination of electrons in TiO_2 matrix with electrolyte. However, it is difficult to obtain a conformal coating of the QD monolayer on the surface of the TiO_2 nanoporous photoelectrode [88]. To increase the coverage ratio of QDs, Lee and co-workers have successively combined the self-assembled monolayer (SAM) and CBD to assemble CdS or CdSe QDs onto the mesoporous TiO_2 electrode [70,75]. The self-assembled CdS QDs on the surface of TiO_2 acted as a seed layer for the enhanced growth of CdS or CdSe in subsequent CBD processes, demonstrated by the higher absorbance shown in Fig. 7b as compared to that in Fig. 7a in the absence of the self-assembled layer of CdS QDs [70]. Comparing the dark currents shown in Fig. 8, this superior deposition of QDs

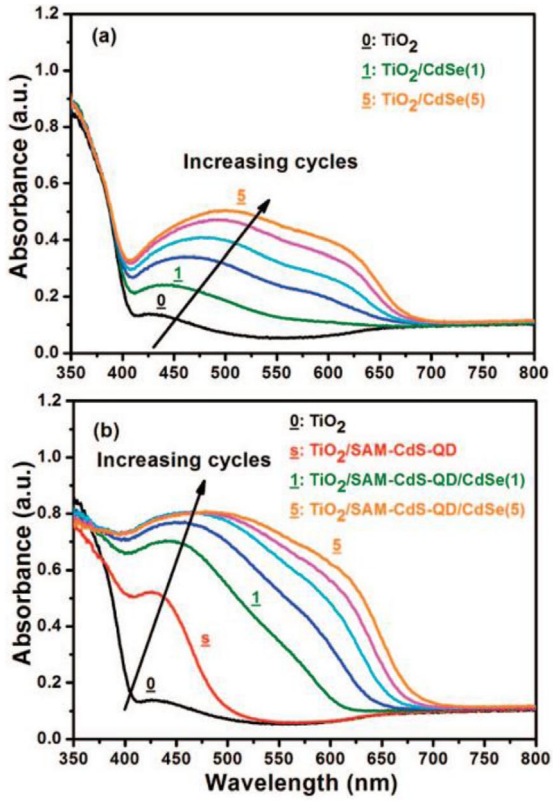

Fig. 7 (Color online) UV–vis absorption spectra of CdSe-sensitized TiO_2 films prepared by various cycles of CBD process in the absence (a) or in the presence (b) of a self-assembled layer of CdS-QD. The number on each curve corresponds to the CBD cycle introduced to assemble the CdSe. (Reprinted with permission from ref. [70]; copyright © 2008, American Chemical Society.)

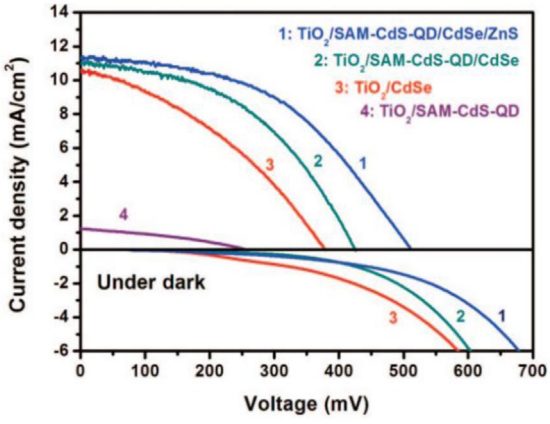

Fig. 8 (Color online) *I–V* characteristics of various QD-sensitized DSSCs measured under the illumination of one sun (AM 1.5, 100 mW/cm^2). The *I–V* characteristics of the cells measured under dark conditions are shown in the lower part of this figure. (Reprinted with permission from ref. [70]; copyright © 2008, American Chemical Society.)

on the TiO_2 surface can inhibit the charge recombination at the TiO_2 electrode/electrolyte interface, leading to an incremental open-circuit potential (V_{OC}) and fill factor (FF) [70]. The obtained open-circuit potential (V_{OC}), short-circuit current (I_{SC}), FF, and total energy conversion efficiency (η) corresponding to these cells are listed in Table 1. All the results indicated that the SAM-CdS-QD layer played an important role in the energy conversion of this kind of solar cell.

Table 1 Parameters obtained from the *I–V* curves of QD-DSSCs using various electrodes. (Reprinted with permission from ref. [70]; copyright © 2008, American Chemical Society.)

Structure	I_{SC} (mA/cm^2)	V_{OC} (mV)	FF	η (%)
TiO_2/SAM-CdS-QD	1.33	260.4	0.33	0.1
TiO_2/CdSe	10.61	378.5	0.36	1.4
TiO_2/SAM-CdS-QD/CdSe	11.00	425.6	0.46	2.1
TiO_2/SAM-CdS-QD/CdS	6.50	459.6	0.47	1.4
TiO_2/SAM-CdS-QD/CdSe/ZnS	11.66	502.6	0.49	2.9

Usually, coating metal oxides (e.g., ZnO, SiO_2, and amorphous TiO_2) with a wide bandgap as a barrier layer on the surface of TiO_2 was proved to be an effective method to enhance the efficiency of QDSCs [17,22,61,71]. Practically, this strategy was also widely used for DSCs, an energy barrier layer between the metal oxide and the dye as a facile and cost-effective method were used to reduce the recombination of photoinjected electrons with redox ions from the electrolyte, including Nb_2O_5 [89,91,92], Al_2O_3 [90,93,94], MgO [95,96], $SrTiO_3$ [97,98], ZrO_2 [97,99], ZnO, SnO_2 [100,101], and TiO_2 [102,103]. This strategy was also used in Cu(In,Ga)Se_2 (CIGS) thin film solar cell to develop the Cd-free buffer layer with improved performance [104–107]. At present, there have been a few reports [17,22,61] about an energy barrier layer between the metal oxide and QDs used in QDSCs. This barrier layer has a higher CB edge than the wide bandgap semiconductor, which can effectively hinder electron back-reactions (R4 process in Fig. 1). Besides, this layer can reduce the interface state density compared to the structure without a barrier layer, in turn suppressing the trapping and recombination of electrons. In practice, the roles of the barrier layer in QDSCs are consistent with theoretical results in CIS-based ETA-solar cells reported by Grasso and Burgelman [108].

Using ZnO as an energy barrier layer coated on the TiO_2 surface in CdS and CdSe-sensitized TiO_2 nanotube solar cells [17,61] has evidently improved the power conversion efficiency. The main reason is that the recombination of injected electrons with holes in QDs and/or in electrolyte was effectively suppressed due to the energy barrier as elaborated above. Recently, Liu and co-workers [22], by using SiO_2 selectively coated on the TiO_2 surface in CdS/CdSe QD co-sensitized solar cells, have obtained a power conversion efficiency of 2.05 % with impressively high IPCE value of 83 %, as shown in Fig. 9. Moreover, the QDSC with SiO_2 coating has longer electron lifetime than that without coating.

All the results demonstrated that wide bandgap metal oxides such as ZnO and SiO_2 as energy barrier layer were able to improve the performance of QDSCs. It is worth noting that the thickness of the barrier layer must be controlled very carefully [60,108]. Theoretically, Grasso and Burgelman [108] have given a curve of short-circuit current J_{SC} of a solar cell with a tunnel interlayer as a function of the layer thickness s (with J_L = 10 mA/cm^2 and V_{OC} = 0.4 V) as shown in Fig. 10, where J_{SC} was steeply descent when s exceeded a critical value, which depended on the barrier height. Therefore, the thickness of the barrier layer must be precisely controlled not to exceed the critical value. Oja Acik's work has also demonstrated the significance of this problem in QDSC performance [60].

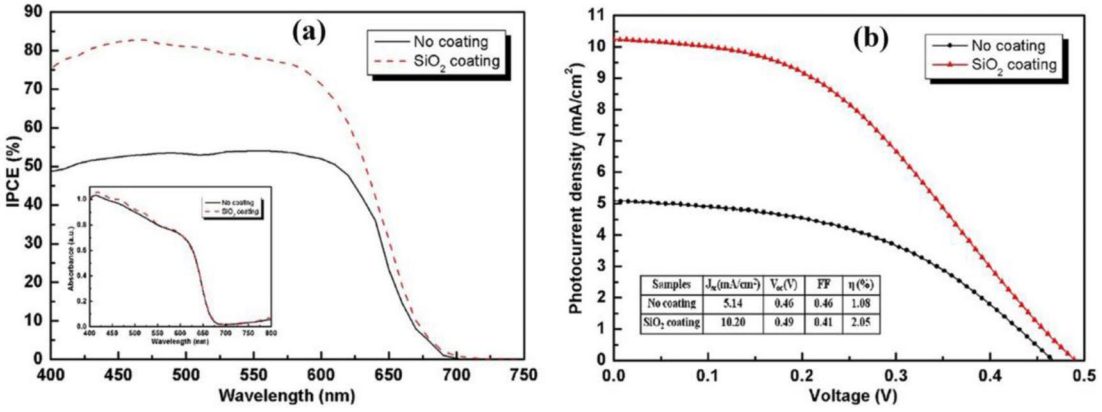

Fig. 9 (Color online) (a) The monochromatic IPCE and the inseted absorption spectra and (b) The *I–V* characteristics (measurements were performed under AM 1.5G, 100 mW/cm^2) of the solar cells based on CdS/CdSe QDs cosensitized electrodes with and without SiO_2 coating. The inset table shows the PV performance of corresponding samples. (Reprinted with permission from ref. [22]; copyright © 2010, American Institute of Physics.)

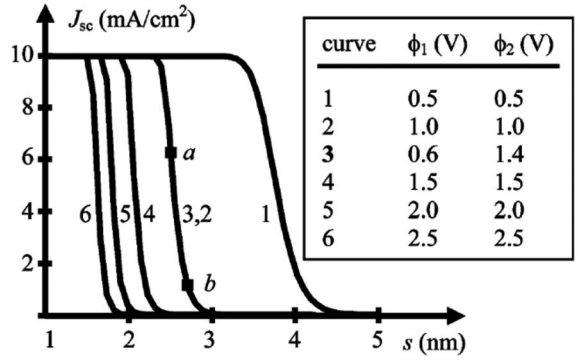

Fig. 10 Short-circuit current of a solar cell with J_L = 10 mA/cm^2 and V_{OC} = 0.4 V with a tunnel interlayer, as a function of the layer width *s*. Barrier heights ϕ_1 and ϕ_2 are indicated in the figure as well. (Reprinted with permission from ref. [108]; copyright © 2004, Elsevier.)

ZnS or amorphous TiO_2 covered on the photoanode surfacing

In the liquid-junction QDSCs, the stability of QDs in electrolyte and serious recombination has to be considered to design this kind of solar cell. Most metal sulfides, except for ZnS, CdS, and CdSe, are unstable in polyiodide electrolyte [109]. Consequently, the nanometric barrier layer between QDs and electrolyte must be included, one of the usual strategies was to use ZnS [3,21,62,67,68,110] and/or amorphous TiO_2 [63,64,71] to at least partially coat the surface of the QD-sensitized electrodes, both the TiO_2 nanoparticles and the QDs (CdSe) [21]. ZnS covering can enhance the stability of QDs in electrolyte and reduce the surface states in QDs and nanostructured TiO_2, which significantly suppresses the surface trapping of photoexcited carriers in QDs and recombination of electrons with redox couple in the electrolyte [3,21,62,111]. Thus, the photoexcited electrons can efficiently transfer into the CB of TiO_2, increase of the electron lifetime and the photocurrent density J_{SC} was obtained [3]. Accordingly, V_{OC} was also enhanced because the quasi-Fermi level in the TiO_2 was moved toward the CB with the increase of the density of electrons injected from the QDs into the CB of TiO_2 photoelectrode [3,87].

The pioneering work by Yang et al. in 2002 proved that a ZnS layer grown by SILAR (successive ionic layer adsorption and reaction) method over a PbS/CdS-sensitized TiO_2 electrode prevented the photocorrosion of chalcogenides and improved the output parameters of the cell [48]. However, this procedure had not received much attention for several years, until Shen and co-workers [62] obtained a high efficiency of 2.02 % by means of this method, almost doubled the efficiencies of CdSe-sensitized solar cells without a ZnS layer. Later, Sixto [110] demonstrated that when the presynthesized CdSe QDs were directly adsorbed on the surface of TiO_2 by a molecular linker, ZnS passivation could also improve the performance of the solar cell. The effect of ZnS passivation on IPCE and current–potential curves under one sun illumination was shown in Fig. 11, where the enhancement effect was much larger for colloidal QDs adsorbed by DA method than that for colloidal QDs deposited using cysteine as the linker molecule [110]. The main reason for this higher performance was that the ZnS surface passivation of TiO_2 reduced the recombination of electrons photoinjected into TiO_2 with the redox couples in the electrolyte, and the same conclusion was derived by Guijarro and co-workers [21].

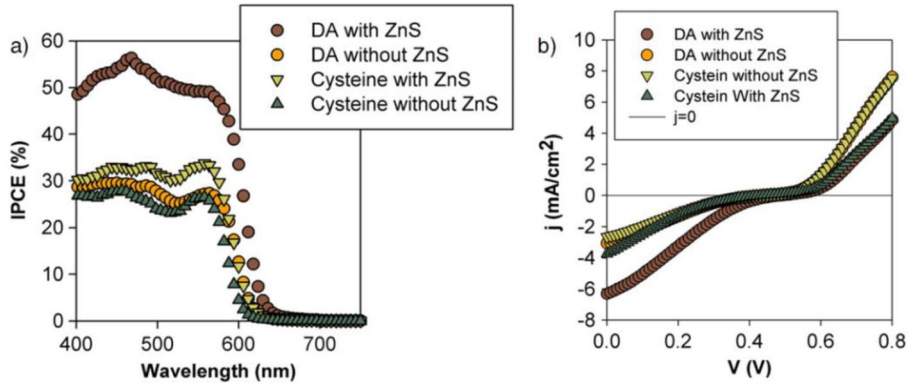

Fig. 11 (Color online) Effect of the ZnS passivation treatment on (a) IPCE and (b) current–potential curves under one sun illumination for a cell configuration: FTO + compact TiO_2 + nanoporous TiO_2 paste + CdSe + polysulfide electrolyte (1 M S) + Pt counter electrode. QD adsorption time: 24 h. (Reprinted with permission from ref. [110]; copyright © 2009, Institute of Physics.)

Unfortunately, a very low FF was attained. Practically, the FF value was usually lower than 0.5, occurred not only in CdSe QD-based solar cells synthesized by CBD method [62], but also in CdSe QDs adsorbed by molecular linkers [110] and CdS/CdSe co-sensitized solar cells [58]. Bisquert's group has tried to explain the reason for this phenomenon via investigating the recombination mechanisms in QDSCs by impedance spectroscopy and open-circuit potential decay measurements [3]. They found the standard exponential rise of the chemical capacitance [112,113] at forward bias plus another feature, a plateau which resulted in the S-shape *I–V* curves under illumination and dark [3], at intermediate potentials for all these electrodes shown in Fig. 12b. On the basis of theories about surface states involved in charge-transport processes [114,115], the plateau feature of the capacitance clearly indicated the presence of surface states that may induce recombination through the monoenergetic level in the bandgap (processes Tr3, R3, and R4 in Fig. 1), causing a strong reduction of the FF and decrease of the energy conversion efficiency of this kind of solar cell [3]. Whatever, the ZnS covering did dramatically enhance the photocurrent and efficiency. To date, using ZnS as a passivation layer to protect QD materials from photocorrosion, the highest energy conversion efficiency achieved has reached 4.22 % for CdS/CdSe co-sensitized TiO_2 solar cell [58].

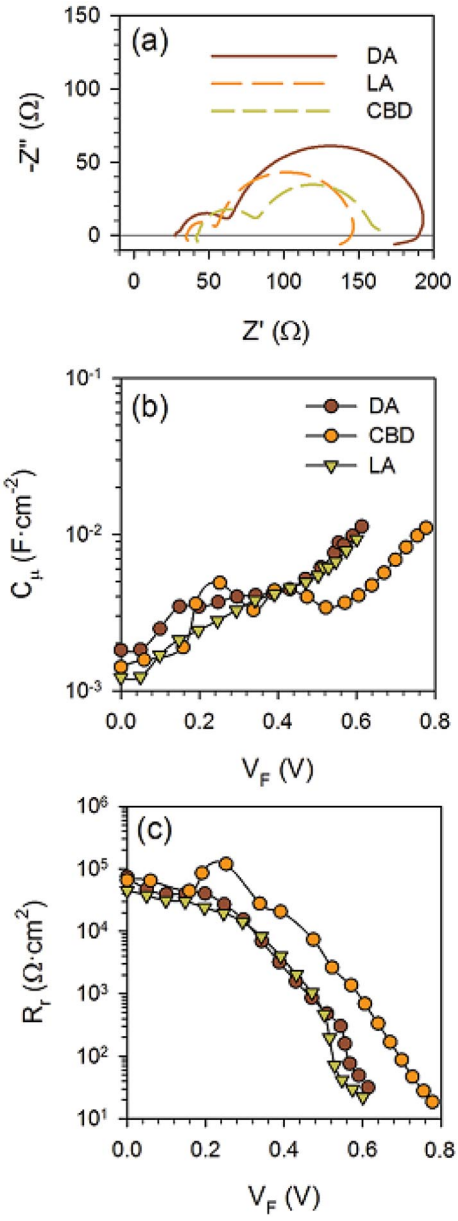

Fig. 12 (Color online) Experimental results of IS of QDSC with configuration FTO + buffer + TiO_2 + QDs + ZnS + polysulfide + Au counter, with QDs deposited by DA, LA, and CBD: (a) impedance spectra at 0.8 V in the dark; (b) chemical capacitance and (c) recombination resistance, as a function of the voltage associated with the second arc of panel a. (Reprinted with permission from ref. [3]; copyright © 2009, American Chemical Society.)

In addition, a thin coating of the QD-sensitized film with an amorphous TiO_2 layer not only had the similar functions to that of ZnS, but also allowed the use of I^-/I^{3-} redox couple, which led to higher V_{OC} and FF (0.6~0.7), compared to the polysulfide electrolyte case [64]. Moreover, an amorphous passivation layer did not induce any stress because of lattice mismatch between the layer and the QDs [116]. So far, a few papers [63,64,71] have reported this approach to improve the performance of QDSCs. Hwang and co-workers have drastically increased the energy conversion efficiency (156 %) of

CdS-sensitized solar cells, using crystalline TiO_2 as a passivation layer, which was synthesized through $TiCl_4$ aqueous solution post-treatment and subsequent thermal annealing [18]. However, the best-obtained photocurrent (5.17 mA/cm^2) was still low. Actually, although an insulating passivation layer indeed impeded the electron back-reaction (desired), at the same time it also hindered the transfer of photoexcited holes toward the electrolyte (undesired) [108], leading to the suppressed photocurrent. Therefore, regardless amorphous or crystalline TiO_2 as a passivation layer, the photocurrents were always low. The recent reports have demonstrated that the $TiCl_4$ treatment did not have a beneficial effect on the photocurrent of QDSCs using TiO_2 nanoparticles [46], but did have a remarkable effect on QDSCs based on SnO_2 spheres acting as electron-conducting media [63].

Molecular dipole adsorption

Many experimental results have proved that the properties of electronic devices could be tuned by desirable molecular dipoles [117–119]. In contrast to linker-connected QDs, this strategy allows QDs to grow directly on the surface of TiO_2, thus the TiO_2/QD interface remains unaffected upon molecular dipole modification. Earlier, Cahen's group has carried out much work to investigate the interaction between molecules and semiconductor surface, and proposed a molecule–surface orbital interaction model based on frontier orbital theory to explain such interactions [117,120,121]. Grafting molecules at the surface of semiconductors (or metals) can shift the CB (or work function), as well as surface states depending on the direction of molecular dipole moments [117,120–122]. This kind of strategy has been used to improve electronic properties of semiconductor surfaces [120,123] as well as the efficiency of various kinds of solar cells [119,124–126], including QDSCs [19,127]. For QDs modified by molecular dipoles, the relative position of the CBs of QDs and TiO_2, together with the recombination resistance R_{rec} has very significant influence on the PV performance. Zaban's [19] and Bisquert's [65] groups have systemically investigated the effect of molecular dipole moments on the *I*–*V* characteristics and the recombination resistance R_{rec} of QDSCs. When the molecular dipole moment was pointing toward QDs, all photocurrent measurements, IPCE and J_{SC}, displayed larger currents for CdS QD-sensitized TiO_2 electrodes [19], as shown in Fig. 13. Meanwhile, the recombination resistance R_{rec} derived from

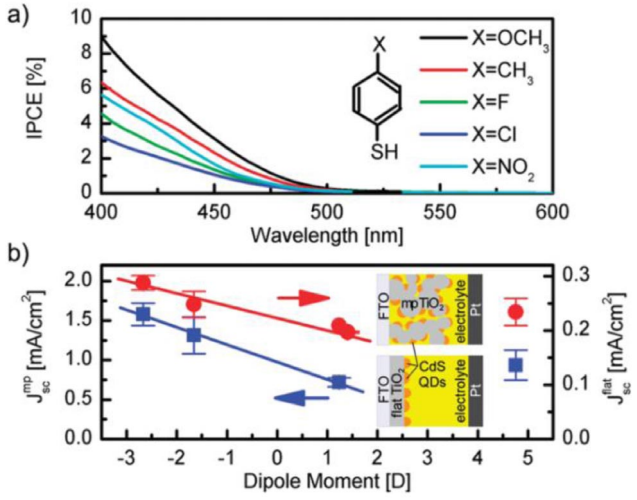

Fig. 13 (Color online) (a) IPCE measurements of CdS QD sensitized flat TiO_2 electrodes, modified with a series of BT derivatives, show a dipole-dependent photoresponse. (b) Dipole-dependent short-circuit current density of flat (●) and mesoporous CdS QD sensitized TiO_2 electrodes (■) measured at AM 1.5G illumination. (Reprinted with permission from ref. [19]; copyright © 2009, American Chemical Society.)

impedance spectroscopy was higher [65], indicating that molecular dipole modification enabled the reduction of the recombination at the electrode/electrolyte interface.

Based on the results from Cahen's group and other related meaningful work [40,117,118,120, 121,123,124,127], Shalom and co-workers [19] have schematically depicted a picture for molecules modified on CdS QDs of different size sensitized on the surface of TiO_2 as shown in Fig. 14. When modified with positive molecular dipole moments (Figs. 14b,e), an energy band diagram showed a downward shift of the energy levels of the QDs, thus electron injection from the lower excited-state energy levels became impossible, leading to the observed lower current density at white light illumination (Fig. 13). In contrary, negative dipoles shifted the energy levels of the QDs upward (Figs. 14c,f), leading to higher photocurrent. Because of the structure differences between the dye and the QDs, one of the challenges is the optimization of the structure of QD/TiO_2 interface for efficient QD $\rightarrow$ TiO_2 electron injection. It has been shown that both thiols [76] and amines [77] bonded strongly to the surface of sulfide particles. Electrons were injected into the CB of TiO_2 at lower excitation energies (Fig. 14c), leading to larger photocurrents at longer wavelengths. Therefore, in this case, electron injection efficiency depended on the molecular dipole, and using molecular dipoles to fine-tune the energy levels of the QDs with respect to an adjacent semiconductor was an important tool for QDSCs and QD-based electronic devices.

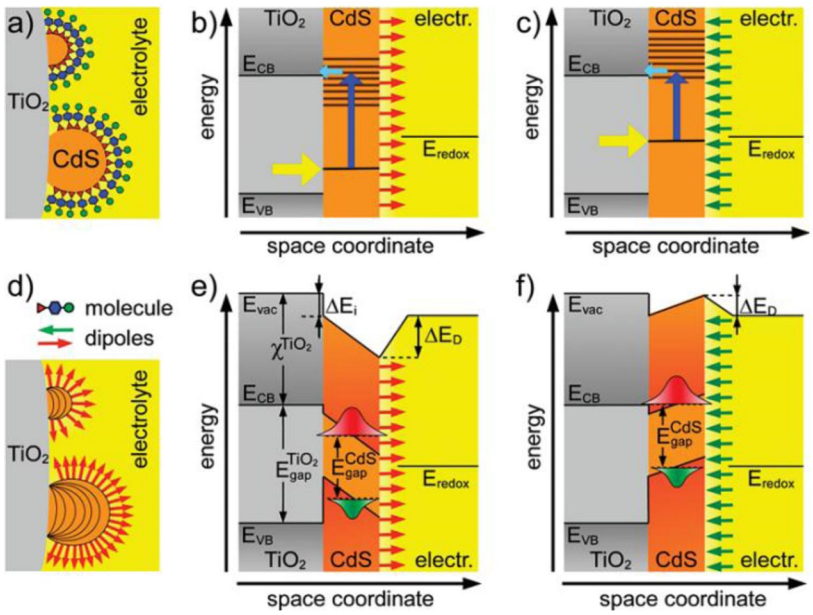

Fig. 14 (Color online) (a) Schematic drawing of sensitized TiO_2 with QDs of different size having a molecular modified surface. (b) Energy band diagram showing the ground and excited states of polydisperse CdS QDs. Molecular dipoles pointing away from the CdS surface shift the QD energy levels down, such that higher photon energies are required (dark blue arrow) to excite electrons into energy states which permit electron injection into the TiO_2 CB (light blue arrow). (c) Negative dipoles shift the QD levels up such that larger QDs, excited at lower photon energies, can also inject electrons into the TiO_2. (d) Schematic drawing of dipole-modified QD surfaces, showing equi-potential lines inside the dots. (e) Energy band diagram of an individual QD, showing the electron affinity χ and the valence and CB edge of TiO_2 (E_{CB} and E_{VB}). The local vacuum level E_{vac} includes an interface dipole ΔE_i at the TiO_2/CdS junction and the potential drop across the dipole layer ΔE_D. The electric field in the QD induced by the molecular dipole layer shifts the electron (red) and hole wave function (green) of the excited state toward lower energies such that electron injection into the TiO_2 is energetically hindered. (f) Negative dipoles shift the energy levels up such that electron injection into the TiO_2 CB becomes possible. (Reprinted with permission from ref. [19]; copyright © 2009, American Chemical Society.)

Ion insertion and surface alloying

It has been known for a long time that the adsorbed inorganic anions and cations at the surface of TiO_2 could influence the photocatalytic processes of illuminated TiO_2 [128]. Researchers have successfully found that surface-fluorinated TiO_2 had enhanced photocatalytic properties [66,129,130]. Soon after this finding, this surface modification method was applied in DSCs to achieve an improved performance [131]. Meanwhile, some researchers have studied the nature of F^- ion adsorption on the surface of TiO_2, and an accepted conclusion was that F^- ion grafted on TiO_2 surface by replacement of some surface hydroxyl groups of TiO_2 and did not induce any etching of TiO_2 particles. More importantly, the Ti–F bond on the surface had an excellent stability against F^- ion back-exchange until pH 12 was reached [46,132,133].

Based on the former work, Diguna has successfully used this strategy in CdSe QD-sensitized TiO_2 for the first time, and the fluoride (F^-) ions were inserted in the interfaces of TiO_2/CdSe and CdSe/ZnS [49]. Comparing electrodes of TiO_2/F/CdSe/F and TiO_2/CdSe, made from a latex template with a diameter of 309 nm, J_{SC} and V_{OC} increased with F^- ion insertion as shown in Fig. 15 and Table 2 [49], and notably, the photoelectric conversion efficiency was doubled. The authors pointed out the different roles of F^- ion insertion in these two interfaces [49]. F^- ions adsorbed on the surface of TiO_2 prior to the deposition of CdSe might take a part in surface passivation, permitting smooth electron transport through TiO_2. On the other hand, regarding the high electronegativity, F^- ion provided the efficient electron guide, whereas electrons from CdSe QDs were pulled toward F^- ions and then transferred to TiO_2. However, further adsorption of F^- ions after the deposition of CdSe led to the formation of CdF_2, performing a similar role as above-mentioned ZnS modification. Regarding the outstanding behavior of F^- ion in QDSCs, Bisquert's group has obtained enhanced efficiencies of different QDSCs, and deeply investigated the origin of the beneficial effect of F^- ion used in CdS, CdSe, and PbS/CdS QD-sensitized TiO_2 solar cells [46]. According to the analysis of impedance spectroscopy [134], the F^- ion could induce a displacement of the TiO_2 CB edge (downward for CdSe and upward for CdS and PbS/CdS), and further affected the recombination processes and the carrier lifetime [43]. These results indicated that a fluorine treatment on the TiO_2 electrodes did lead to a general improvement of the performance of QDSCs, regardless of the light-absorbing materials used in QDSCs, and provided a new design methodology for high-efficiency QDSCs.

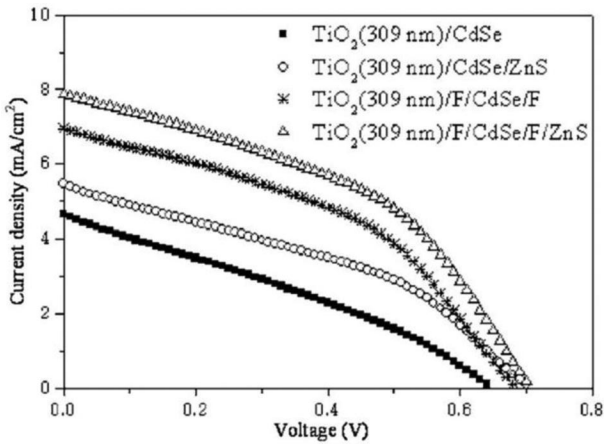

Fig. 15 *J–V* characteristic of four different TiO_2 inverse opal electrodes made from a latex template with a diameter of 309 nm (TiO_2/CdSe, TiO_2/CdSe/ZnS, TiO_2/F/CdSe/F, and TiO_2/F/CdSe/F/ZnS), measured using a solar simulator (Peccell technologies, Inc.) with 100 mW/cm^2 irradiation (AM 1.5). (Reprinted with permission from ref. [49]; copyright © 2007, American Institute of Physics.)

Table 2 PV properties of different TiO_2 inverse opal electrodes made from latex templates of 309 and 394 nm in diameter. (Reprinted with permission from ref. [49]; copyright © 2007, American Institute of Physics.)

Electrode	J_{SC} (mA/cm^2)	V_{OC} (mV)	FF	η (%)
	Latex diameter of 309 nm			
TiO_2/CdSe	4.65	0.65	0.31	0.9
TiO_2/CdSe/ZnS	5.48	0.71	0.38	1.5
TiO_2/F/CdSe/F	6.95	0.69	0.42	2.0
TiO_2/F/CdSe/F/ZnS	7.87	0.71	0.44	2.4
	Latex diameter of 394 nm			
TiO_2/CdSe	6.03	0.68	0.39	1.6
TiO_2/F/CdSe/F/ZnS	7.51	0.71	0.50	2.7

Recently, another surface modification has been proposed in addition to the fluorine ion insertion. Spray et al. reported that alloying of Fe_2O_3 photoelectrode by adsorbing Al^{3+} or Sn^{4+} ions on the surface followed by annealing dramatically improved the photoresponse [135]. The role of the alloying process was believed to be a similar coating layer to remove surface states and suppress back-reactions.

Therefore, it seems that not only a compound could passivate the interface, but also cations and anions could selectively saturate dangling bonds and remove surface states in the interface. Theoretical modeling is, however, needed to resolve the exact structural and electronic transformation during and after the modification.

Inserting n-type transition-metal oxide (MoO_x, V_2O_x) layer between the QD film and the top-contact anode

The approach based on a transition-metal oxide (TMO) as hole extraction layer (HEL) was used previously in organic light-emitting diodes (LEDs) [136,137] and organic solar cells [138–142], having obtained satisfactory results with a merit that contamination by air exposure did not significantly affect its hole transport property [143]. Usually, TMO was made by thermal evaporation at an oxygen-deficient environment [144], and for simplicity, the notations of MoO_x and V_2O_x were used to represent the non-stoichiometry of thermally evaporated TMO films. Considering the similar working principle of organic solar cells and QDSCs, some researchers have introduced MoO_x as the HEL between the QD film and the top-contact anode to improve the power conversion efficiency of QDSCs [16,47]. So far, ZnO/PbS QD heterojunction PVs have reached the highest-efficiency of 4.4 % certified by NREL [47]. Figure 16b clearly showed the effect of the HEL on the *J–V* characteristics of different devices, with all device parameters being listed in Table 3 [47]. Because of the Schottky junction formed by the metal contact [16] as shown in Fig. 16a [47], photogenerated holes accumulated at the interface of PbS QDs/anode, while electrons could be collected in both directions (by anode or cathode), causing increased recombination at the anode [16], further limiting both the dark current and the photocurrent in forward bias and reducing the V_{OC}, resulted in a roll-over effect [145] above the V_{OC} in the *J–V* curves for Al, Ag, or Au contact. By inserting MoO_x layer, the roll-over was eliminated for Al contact, corresponding to higher FF, V_{OC}, and J_{SC}. Similar *J–V* characteristics were observed for Au and Ag contacts [16]. A two-diode model fitting results revealed that inserting MoO_x completely removed the back-diode, and as shown in Fig. 16b, the hole barrier height reduced from more than 0.60 eV for all contacts to 0 eV by inserting MoO_x as the HEL. All device parameters listed in Table 3 indicated that with the HEL the device performance was independent of the anode material, in contrast to the cases without the HEL. Furthermore, it can be concluded that the hole extraction mechanism depended only on the PbS/MoO_x interface, instead of the MoO_x/metal anode interface [138,139].

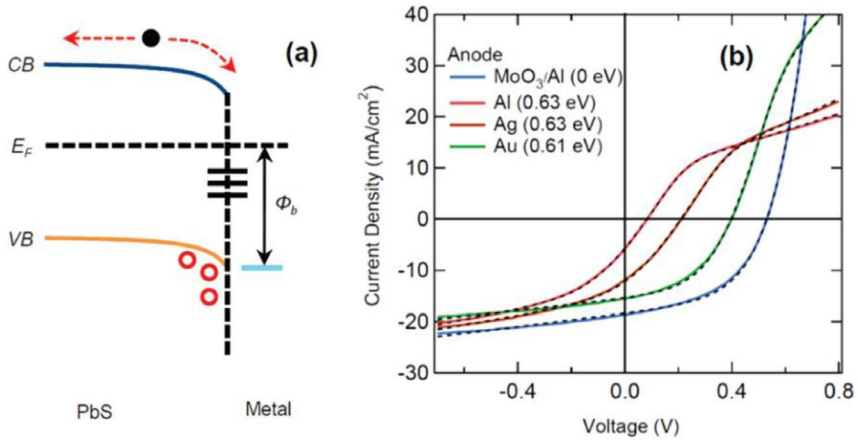

Fig. 16 (Color online) (a) Schematic energy diagram of the unintentional Schottky diode at the PbS/metal interface. (b) Measured light *J*–*V* characteristics under 100 mW/cm^2 white light illumination for devices with various anodes (solid lines). The dotted lines are fitting curves based on a two-diode model. The values in parentheses are the fitting results of Schottky junction hole injection barrier height. (Reprinted with permission from ref. [47]; copyright © 2011, American Chemical Society.)

Table 3 PbS QD solar cell operation parameters for devices with various anodes. (Reprinted with permission from ref. [47]; copyright © 2011, American Chemical Society.)

Anode	V_{OC} (mV)	J_{SC} (mA/cm^2)	FF	PCE (%)
10 nm MoO_x/Al	524.5	17.9	48.7	4.46
20 nm MoO_x/Al	549.5	17.9	41.5	4.20
10 nm MoO_x/Ag	530.4	18.7	47.6	4.53
10 nm MoO_x/Au	540.0	17.4	47.0	4.41
10 nm V_2O_x/Al	525.8	19.1	44.8	4.48
Al	83.8	5.6	26.0	0.12
Ag	212.1	11.4	30.2	0.73
Au	399.5	15.5	43	2.66

The dominating reason for the significant PCE increase with the insertion of the MoO_x layer was that the high-work-function MoO_x film pinned the Fermi level of the anode contact and prevented the formation of a Schottky junction [16]. Gao et al. have further studied the nature of PbS/MoO_x interface by UV photoemission spectroscopy (UPS) to determine the interfacial energy levels between MoO_x and PbS QD layer [47]. The UPS data of a PbS film without and with 10 nm MoO_x and the deduced schematic energy diagram for the PbS/MoO_x interface were shown in Figs. 17a,b, respectively [47]. Upon depositing 10 nm MoO_x, the work function increased by 0.63 eV, and the resulting interfacial dipole enhanced the band bending at the interface between the MoO_x and PbS QD layer, allowing more efficient hole collection at the PbS/MoO_x interface, which was proposed to occur also in the MoO_x/organic interface [146,147]. Furthermore, the shallow gap states owing to oxygen vacancy in MoO_x deduced from the UPS data as shown in the right panel of Fig. 17a nearly aligned with the valence band of PbS layer at the PbS/MoO_x interface, which might contribute to the efficient hole extraction.

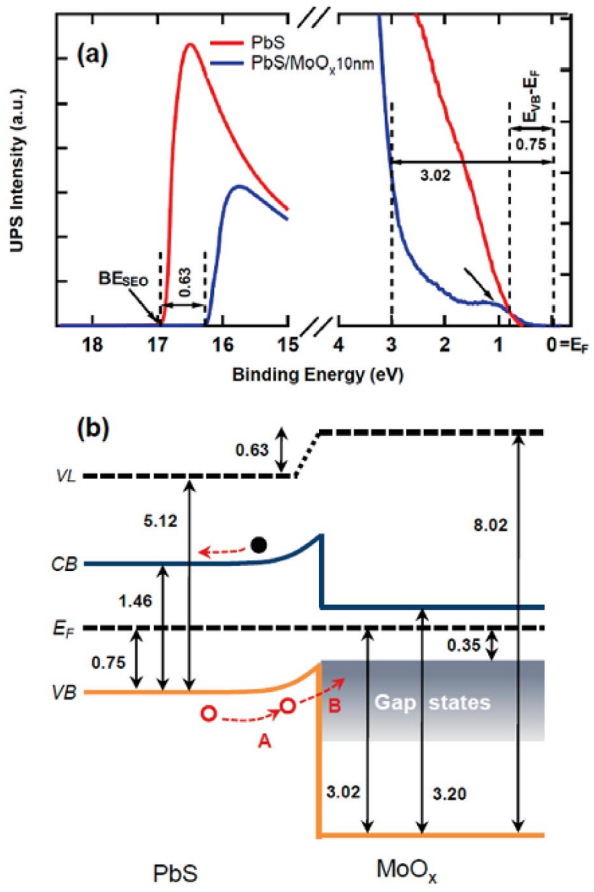

Fig. 17 (Color online) (a) UPS cutoff spectra of PbS and PbS/MoO_x. Left panel is the work function and right panel is the valence band region, respectively. The work function is calculated by subtracting the secondary emission binding energy offset (BESEO) from excitation beam (21.2 eV) and the energy difference between VB to Fermi level is calculated by the linear portion of the low binding energy side of the proper VB peak relative to the energy axis. (b) Schematic energy diagram of interfacial layers PbS/MoO_x deduced by the UPS data in panel (a). PbS QD and MoO_x bandgap are 1.46 eV from PbS thin film optical absorption spectrum and 3.2 eV from literature [*Org. Electron.* **11**, 188 (2010)], respectively. (Reprinted with permission from ref. [47]; copyright © 2011, American Chemical Society.)

The above main findings demonstrate that this strategy not only offers the opportunity to replace the high-work-function metal Au anode contact with TMO/Al while maintaining device performance [47], but also allows for the use of a transparent ITO top electrode to optically probe the different device interfaces during operation [16].

FINAL REMARKS

In recent years, nanostructured solar cells, as the third-generation device, have evolved rapidly from basic concepts to realistic power converters with high efficiency. The device performance depends on the sequential processes of charge dissociation, transport, and collection. The interfacial contact plays a central role in the charge-transport and collection dynamics. Some common strategies for interface engineering are highlighted. In practical applications, two promising strategies can be combined in the

device design, such as insertion F^- ion and passivation of ZnS [46,49], to get more satisfying results. It is worth pointing out that the same passivation material at different interfaces of two differing materials could play dramatically different roles, for example, we have shown in a recent publication that ZnS could function as a physical blocking layer between TiO_2 electrode and $CuInS_2$ absorber whereas as an electric field modifier between CdS and sulfide electrolyte [148]. As we have pointed out above, some of the strategies listed here were similar to those adopted in DSCs or organic solar cells, and these interface modifications have greatly increased the photocurrent, photovoltage, and energy conversion efficiency of nanostructured solar cells. The optimization of the electrical contacts is as important as the other relevant techniques in the device design, such as modification of the polysulfide electrolyte [26,59], finding a more proper counter electrode [149], and optimization of the TiO_2 semiconductor topography [150]. A better understanding and control of the interface properties of nanostructured solar cells will allow us to derive a general design rule to engineer future material systems for a better energy conversion efficiency and realistic PV applications.

ACKNOWLEDGMENTS

This work was supported by the National Basic Research Program of China (973 Program, Grant No. 2011CB302103), the Natural Science Foundation of China (Grant Nos. 10874183 and 11074255), and the Hundred Talent Program of the Chinese Academy of Sciences.

REFERENCES

1. F. Sauvage, D. Chen, P. Comte, F. Huang, L.-P. Heiniger, Y.-B. Cheng, R. A. Caruso, M. Graetzel. *ACS Nano* **4**, 4420 (2010).
2. O. Shevaleevskiy. *Pure Appl. Chem.* **80**, 2079 (2008).
3. I. Mora-Sero, S. Gimenez, F. Fabregat-Santiago, R. Gomez, Q. Shen, T. Toyoda, J. Bisquert. *Acc. Chem. Res.* **42**, 1848 (2009).
4. W. Lee, J. Lee, S. Lee, W. Yi, S. H. Han, B. W. Cho. *Appl. Phys. Lett.* **92**, 153510 (2008).
5. L. L. Yin, C. H. Ye. *Sci. Adv. Mater.* **3**, 41 (2011).
6. I. Mora-Sero, S. Gimenez, F. Fabregat-Santiago, E. Azaceta, R. Tena-Zaera, J. Bisquert. *Phys. Chem. Chem. Phys.* **13**, 7162 (2011).
7. J. M. Luther, M. Law, M. C. Beard, Q. Song, M. O. Reese, R. J. Ellingson, A. J. Nozik. *Nano Lett.* **8**, 3488 (2008).
8. A. G. Pattantyus-Abraham, I. J. Kramer, A. R. Barkhouse, X. Wang, G. Konstantatos, R. Debnath, L. Levina, I. Raabe, M. K. Nazeeruddin, M. Graetzel, E. H. Sargent. *ACS Nano* **4**, 3374 (2010).
9. D. A. R. Barkhouse, R. Debnath, I. J. Kramer, D. Zhitomirsky, A. G. Pattantyus-Abraham, L. Levina, L. Etgar, M. Graetzel, E. H. Sargent. *Adv. Mater.* **23**, 3134 (2011).
10. J. Jortner, C. N. R. Rao. *Pure Appl. Chem.* **74**, 1491 (2002).
11. W. W. Yu, L. Qu, W. Guo, X. Peng. *Chem. Mater.* **15**, 2854 (2003).
12. W. W. Yu, X. Peng. *Angew. Chem., Int. Ed.* **41**, 2368 (2002).
13. R. Vogel, P. Hoyer, H. Weller. *J. Phys. Chem.* **98**, 3183 (1994).
14. P. V. Kamat. *J. Phys. Chem. C* **112**, 18737 (2008).
15. B.-R. Hyun, A. C. Bartnik, L. Sun, T. Hanrath, F. W. Wise. *Nano Lett.* **11**, 2126 (2011).
16. P. R. Brown, R. R. Lunt, N. Zhao, T. P. Osedach, D. D. Wanger, L.-Y. Chang, M. G. Bawendi, V. Bulovic. *Nano Lett.* **11**, 2955 (2011).
17. C. Chen, Y. Xie, G. Ali, S. Yoo, S. Cho. *Nanotechnology* **22**, 015202 (2011).
18. J.-Y. Hwang, S.-A. Lee, Y. H. Lee, S.-I. Seok. *ACS Appl. Mater. Interfaces* **2**, 1343 (2010).
19. M. Shalom, S. Ruehle, I. Hod, S. Yahav, A. Zaban. *J. Am. Chem. Soc.* **131**, 9876 (2009).

20. W.-T. Sun, Y. Yu, H.-Y. Pan, X.-F. Gao, Q. Chen, L.-M. Peng. *J. Am. Chem. Soc.* **130**, 1124 (2008).
21. N. Guijarro, J. M. Campina, Q. Shen, T. Toyoda, T. Lana-Villarreal, R. Gomez. *Phys. Chem. Chem. Phys.* **13**, 12024 (2011).
22. Z. Liu, M. Miyauchi, Y. Uemura, Y. Cui, K. Hara, Z. Zhao, K. Sunahara, A. Furube. *Appl. Phys. Lett.* **96**, 233107 (2010).
23. S. H. Im, H.-J. Kim, J. H. Rhee, C.-S. Lim, S. I. Seok. *Energy Environ. Sci.* **4**, 2799 (2011).
24. Y. Itzhaik, O. Niitsoo, M. Page, G. Hodes. *J. Phys. Chem. C* **113**, 4254 (2009).
25. I. Robel, V. Subramanian, M. Kuno, P. V. Kamat. *J. Am. Chem. Soc.* **128**, 2385 (2006).
26. L. Li, X. Yang, J. Gao, H. Tian, J. Zhao, A. Hagfeldt, L. Sun. *J. Am. Chem. Soc.* **133**, 8458 (2011).
27. R. Al-Salman, X. Meng, J. Zhao, Y. Li, U. Kynast, M. M. Lezhnina, F. Endres. *Pure Appl. Chem.* **82**, 1673 (2010).
28. J. L. Blackburn, D. C. Selmarten, R. J. Ellingson, M. Jones, O. Micic, A. J. Nozik. *J. Phys. Chem. B* **109**, 2625 (2005).
29. P. Yu, K. Zhu, A. G. Norman, S. Ferrere, A. J. Frank, A. J. Nozik. *J. Phys. Chem. B* **110**, 25451 (2006).
30. R. D. Schaller, V. I. Klimov. *Phys. Rev. Lett.* **92**, 186601 (2004).
31. D. J. Binks. *Phys. Chem. Chem. Phys.* **13**, 12693 (2011).
32. B. O'Regan, M. Graetzel. *Nature* **353**, 737 (1991).
33. S. S. Kale, R. S. Mane, C. D. Lokhande, K. C. Nandi, S. H. Han. *Mater. Sci. Eng. B* **133**, 222 (2006).
34. V. Gonzalez-Pedro, X. Xu, I. Mora-Sero, J. Bisquert. *ACS Nano* **4**, 5783 (2010).
35. V. Chakrapani, D. Baker, P. V. Kamat. *J. Am. Chem. Soc.* **133**, 9607 (2011).
36. I. Mora-Sero, S. Gimenez, T. Moehl, F. Fabregat-Santiago, T. Lana-Villareal, R. Gomez, J. Bisquert. *Nanotechnology* **19**, 424007 (2008).
37. S. B. Patil, A. K. Singh. *Electrochim. Acta* **56**, 5693 (2011).
38. J. H. Bang, P. V. Kamat. *ACS Nano* **3**, 1467 (2009).
39. J. Tornow, K. Schwarzburg, A. Belaidi, T. Dittrich, M. Kunst, T. Hannappel. *J. Appl. Phys.* **108**, 044915 (2010).
40. D. Cahen, A. Kahn. *Adv. Mater.* **15**, 271 (2003).
41. I. Mora-Sero, J. Bisquert. *J. Phys. Chem. Lett.* **1**, 3046 (2010).
42. A. P. Alivisatos. *Science* **271**, 933 (1996).
43. G. Boschloo, D. Fitzmaurice. *J. Phys. Chem. B* **103**, 2228 (1999).
44. C.-Y. Chen, M.-W. Chen, J.-J. Ke, C.-A. Lin, J. R. D. Retamal, J.-H. He. *Pure Appl. Chem.* **82**, 2055 (2010).
45. L. Kronik, Y. Shapira. *Surf. Sci. Rep.* **37**, 1 (1999).
46. M. Samadpour, P. P. Boix, S. Gimenez, A. I. Zad, N. Taghavinia, I. Mora-Sero, J. Bisquert. *J. Phys. Chem. C* **115**, 14400 (2011).
47. J. Gao, C. L. Perkins, J. M. Luther, M. C. Hanna, H.-Y. Chen, O. E. Semonin, A. J. Nozik, R. J. Ellingson, M. C. Beard. *Nano Lett.* **11**, 3263 (2011).
48. S.-M. Yang, C.-H. Huang, J. Zhai, Z.-S. Wang, L. Jiang. *J. Mater. Chem.* **12**, 1459 (2002).
49. L. J. Diguna, Q. Shen, J. Kobayashi, T. Toyoda. *Appl. Phys. Lett.* **91**, 023116 (2007).
50. D. Lawless, S. Kapoor, D. Meisel. *J. Phys. Chem.* **99**, 10329 (1995).
51. K. S. Leschkies, R. Divakar, J. Basu, E. Enache-Pommer, J. E. Boercker, C. B. Carter, U. R. Kortshagen, D. J. Norris, E. S. Aydil. *Nano Lett.* **7**, 1793 (2007).
52. L. M. Peter, D. J. Riley, E. J. Tull, K. G. U. Wijayantha. *Chem. Commun.* 1030 (2002).
53. S. Yu-Jen, L. Yuh-Lang. *Nanotechnology* **19**, 045602 (2008).
54. P. Szymanski, N. Fuke, A. Y. Koposov, V. W. Manner, L. B. Hoch, M. Sykora. *Chem. Commun.* **47**, 6437 (2011).

55. O. Niitsoo, S. K. Sarkar, C. Pejoux, S. Rühle, D. Cahen, G. Hodes. *J. Photochem. Photobiol., A* **181**, 306 (2006).
56. Y. F. Nicolau. *Appl. Surf. Sci.* **22–23**, 1061 (1985).
57. S. Gorer, G. Hodes. *J. Phys. Chem.* **98**, 5338 (1994).
58. Y.-L. Lee, Y.-S. Lo. *Adv. Funct. Mater.* **19**, 604 (2009).
59. C.-Y. Chou, C.-P. Lee, R. Vittal, K.-C. Ho. *J. Power Sources* **196**, 6595 (2011).
60. I. Oja Acik, A. Katerski, A. Mere, J. Aarik, A. Aidla, T. Dedova, M. Krunks. *Thin Solid Films* **517**, 2443 (2009).
61. W. Lee, S. H. Kang, J.-Y. Kim, G. B. Kolekar, Y.-E. Sung, S.-H. Han. *Nanotechnology* **20**, 335706 (2009).
62. Q. Shen, J. Kobayashi, L. J. Diguna, T. Toyoda. *J. Appl. Phys.* **103**, 084304 (2008).
63. M. A. Hossain, G. Yang, M. Parameswaran, J. R. Jennings, Q. Wang. *J. Phys. Chem. C* **114**, 21878 (2010).
64. M. Shalom, S. Dor, S. Ruehle, L. Grinis, A. Zaban. *J. Phys. Chem. C* **113**, 3895 (2009).
65. E. M. Barea, M. Shalom, S. Gimenez, I. Hod, I. Mora-Sero, A. Zaban, J. Bisquert. *J. Am. Chem. Soc.* **132**, 6834 (2010).
66. H. Park, W. Choi. *J. Phys. Chem. B* **108**, 4086 (2004).
67. J. Reichman, M. A. Russak. *J. Appl. Phys.* **53**, 708 (1982).
68. S. A. Wessel, K. Colbow. *Semicond. Sci. Tech.* **2**, 747 (1987).
69. I. Gur, N. A. Fromer, M. L. Geier, A. P. Alivisatos. *Science* **310**, 462 (2005).
70. Y.-L. Lee, B.-M. Huang, H.-T. Chien. *Chem. Mater.* **20**, 6903 (2008).
71. H. Yang, C. Guo, G. H. Guai, Q. Song, S. P. Jiang, C. M. Li. *ACS Appl. Mater. Interfaces* **3**, 1940 (2011).
72. A. Kongkanand, K. Tvrdy, K. Takechi, M. Kuno, P. V. Kamat. *J. Am. Chem. Soc.* **130**, 4007 (2008).
73. R. S. Dibbell, D. F. Watson. *J. Phys. Chem. C* **113**, 3139 (2009).
74. R. S. Dibbell, D. G. Youker, D. F. Watson. *J. Phys. Chem. C* **113**, 18643 (2009).
75. S. C. Lin, Y. L. Lee, C. H. Chang, Y. J. Shen, Y. M. Yang. *Appl. Phys. Lett.* **90**, 143517 (2007).
76. V. Swayambunathan, D. Hayes, K. H. Schmidt, Y. X. Liao, D. Meisel. *J. Am. Chem. Soc.* **112**, 3831 (1990).
77. T. Dannhauser, M. O'Neil, K. Johansson, D. Whitten, G. McLendon. *J. Phys. Chem.* **90**, 6074 (1986).
78. S. Logunov, T. Green, S. Marguet, M. A. El-Sayed. *J. Phys. Chem. A* **102**, 5652 (1998).
79. Y. Nosaka, H. Miyama, M. Terauchi, T. Kobayashi. *J. Phys. Chem.* **92**, 255 (1988).
80. I. Robel, M. Kuno, P. V. Kamat. *J. Am. Chem. Soc.* **129**, 4136 (2007).
81. S. F. Wuister, C. de Mello Donega, A. Meijerink. *J. Phys. Chem. B* **108**, 17393 (2004).
82. V. V. Breus, C. D. Heyes, G. U. Nienhaus. *J. Phys. Chem. C* **111**, 18589 (2007).
83. T. Rajh, A. E. Ostafin, O. I. Micic, D. M. Tiede, M. C. Thurnauer. *J. Phys. Chem.* **100**, 4538 (1996).
84. D. J. Norris, M. G. Bawendi. *Phys. Rev. B* **53**, 16338 (1996).
85. K. Tvrdy, P. A. Frantsuzov, P. V. Kamat. *Proc. Natl. Acad. Sci. USA* **108**, 29 (2011).
86. G. Hodes. *J. Phys. Chem. C* **112**, 17778 (2008).
87. J. Bisquert, A. Zaban, P. Salvador. *J. Phys. Chem. B* **106**, 8774 (2002).
88. S. Rawalekar, S. Kaniyankandy, S. Verma, H. N. Ghosh. *J. Phys. Chem. C* **115**, 12335 (2011).
89. A. Zaban, S. G. Chen, S. Chappel, B. A. Gregg. *Chem. Commun.* 2231 (2000).
90. X.-T. Zhang, H.-W. Liu, T. Taguchi, Q.-B. Meng, O. Sato, A. Fujishima. *Sol. Energy Mater. Sol. Cells* **81**, 197 (2004).
91. E. Barea, X. Xu, V. Gonzalez-Pedro, T. Ripolles-Sanchis, F. Fabregat-Santiago, J. Bisquert. *Energy Environ. Sci.* **4**, 3414 (2011).
92. S. G. Chen, S. Chappel, Y. Diamant, A. Zaban. *Chem. Mater.* **13**, 4629 (2001).

93. M. Law, L. E. Greene, A. Radenovic, T. Kuykendall, J. Liphardt, P. Yang. *J. Phys. Chem. B* **110**, 22652 (2006).
94. E. Palomares, J. N. Clifford, S. A. Haque, T. Lutz, J. R. Durrant. *J. Am. Chem. Soc.* **125**, 475 (2003).
95. G. R. A. Kumara, M. Okuya, K. Murakami, S. Kaneko, V. V. Jayaweera, K. Tennakone. *J. Photochem. Photobiol., A* **164**, 183 (2004).
96. H. S. Jung, J.-K. Lee, M. Nastasi, S.-W. Lee, J.-Y. Kim, J.-S. Park, K. S. Hong, H. Shin. *Langmuir* **21**, 10332 (2005).
97. Y. Diamant, S. Chappel, S. G. Chen, O. Melamed, A. Zaban. *Coord. Chem. Rev.* **248**, 1271 (2004).
98. Y. Diamant, S. G. Chen, O. Melamed, A. Zaban. *J. Phys. Chem. B* **107**, 1977 (2003).
99. J. Kim, S. Lee, J. Noh, H. Jung, K. Hong. *J. Electroceram.* **23**, 422 (2009).
100. K. M. P. Bandaranayake, M. K. Indika Senevirathna, P. M. G. M. Prasad Weligamuwa, K. Tennakone. *Coord. Chem. Rev.* **248**, 1277 (2004).
101. K. E. Kim, S.-R. Jang, J. Park, R. Vittal, K.-J. Kim. *Sol. Energy Mater. Sol. Cells* **91**, 366 (2007).
102. P. M. Sommeling, B. C. O'Regan, R. R. Haswell, H. J. P. Smit, N. J. Bakker, J. J. T. Smits, J. M. Kroon, J. A. M. van Roosmalen. *J. Phys. Chem. B* **110**, 19191 (2006).
103. B. C. O'Regan, J. R. Durrant, P. M. Sommeling, N. J. Bakker. *J. Phys. Chem. C* **111**, 14001 (2007).
104. B. T. Ahn, L. Larina, K. H. Kim, S. J. Ahn. *Pure Appl. Chem.* **80**, 2091 (2008).
105. T. Nakada, M. Mizutani, Y. Hagiwara, A. Kunioka. *Sol. Energy Mater. Sol. Cells* **67**, 255 (2001).
106. Y. Ohtake, T. Okamoto, A. Yamada, M. Konagai, K. Saito. *Sol. Energy Mater. Sol. Cells* **49**, 269 (1997).
107. N. Naghavi, S. Spiering, M. Powalla, B. Cavana, D. Lincot. *Prog. Photovolt.* **11**, 437 (2003).
108. C. Grasso, M. Burgelman. *Thin Solid Films* **451–452**, 156 (2004).
109. A. B. Ellis, S. W. Kaiser, J. M. Bolts, M. S. Wrighton. *J. Am. Chem. Soc.* **99**, 2839 (1977).
110. S. Gimenez, I. Mora-Sero, L. Macor, N. Guijarro, T. Lana-Villarreal, R. Gomez, L. J. Diguna, Q. Shen, T. Toyoda, J. Bisquert. *Nanotechnology* **20**, 295204 (2009).
111. A. Braga, S. Gimenez, I. Concina, A. Vomiero, I. Mora-Sero. *J. Phys. Chem. Lett.* **2**, 454 (2011).
112. J. Bisquert. *Phys. Chem. Chem. Phys.* **5**, 5360 (2003).
113. J. Bisquert, F. Fabregat-Santiago, I. Mora-Sero, G. Garcia-Belmonte, E. M. Barea, E. Palomares. *Inorg. Chim. Acta* **361**, 684 (2008).
114. I. Mora-Sero, J. Bisquert. *Nano Lett.* **3**, 945 (2003).
115. I. Abayev, A. Zaban, V. G. Kytin, A. A. Danilin, G. Garcia-Belmonte, J. Bisquert. *J. Solid State Electrochem.* **11**, 647 (2007).
116. A. Hultqvist, M. Edoff, T. Torndahl. *Prog. Photovolt.* **19**, 478 (2011).
117. A. Vilan, A. Shanzer, D. Cahen. *Nature* **404**, 166 (2000).
118. D. Gal, E. Sone, R. Cohen, G. Hodes, J. Libman, A. Shanzer, H. W. Schock, D. Cahen. *Proc. Ind. Acad. Sci. Chem. Sci.* **109**, 487 (1997).
119. I. H. Campbell, J. D. Kress, R. L. Martin, D. L. Smith, N. N. Barashkov, J. P. Ferraris. *Appl. Phys. Lett.* **71**, 3528 (1997).
120. R. Cohen, L. Kronik, A. Vilan, A. Shanzer, D. Cahen. *Adv. Mater.* **12**, 33 (2000).
121. G. Ashkenasy, D. Cahen, R. Cohen, A. Shanzer, A. Vilan. *Acc. Chem. Res.* **35**, 121 (2002).
122. M. Soreni-Harari, N. Yaacobi-Gross, D. Steiner, A. Aharoni, U. Banin, O. Millo, N. Tessler. *Nano Lett.* **8**, 678 (2008).
123. R. Cohen, L. Kronik, A. Shanzer, D. Cahen, A. Liu, Y. Rosenwaks, J. K. Lorenz, A. B. Ellis. *J. Am. Chem. Soc.* **121**, 10545 (1999).
124. H. Haick, J. Ghabboun, O. Niitsoo, H. Cohen, D. Cahen, A. Vilan, J. Hwang, A. Wan, F. Amy, A. Kahn. *J. Phys. Chem. B* **109**, 9622 (2005).
125. S. Khodabakhsh, B. M. Sanderson, J. Nelson, T. S. Jones. *Adv. Funct. Mater.* **16**, 95 (2006).

126. N. R. Neale, N. Kopidakis, J. van de Lagemaat, M. Graetzel, A. J. Frank. *J. Phys. Chem. B* **109**, 23183 (2005).
127. I. Visoly-Fisher, A. Sitt, M. Wahab, D. Cahen. *Chemphyschem* **6**, 277 (2005).
128. M. Abdullah, G. K. C. Low, R. W. Matthews. *J. Phys. Chem.* **94**, 6820 (1990).
129. J. Tang, H. Quan, J. Ye. *Chem. Mater.* **19**, 116 (2007).
130. K. Lv, Y. Xu. *J. Phys. Chem. B* **110**, 6204 (2006).
131. X. F. Cheng, W. H. Leng, D. P. Liu, Y. M. Xu, J. Q. Zhang, C. N. Cao. *J. Phys. Chem. C* **112**, 8725 (2008).
132. M. Minella, M. G. Faga, V. Maurino, C. Minero, E. Pelizzetti, S. Coluccia, G. Martra. *Langmuir* **26**, 2521 (2010).
133. C. Minero, G. Mariella, V. Maurino, E. Pelizzetti. *Langmuir* **16**, 2632 (2000).
134. F. Fabregat-Santiago, G. Garcia-Belmonte, I. Mora-Sero, J. Bisquert. *Phys. Chem. Chem. Phys.* **13**, 9083 (2011).
135. R. L. Spray, K. J. McDonald, K.-S. Choi. *J. Phys. Chem. C* **115**, 3497 (2011).
136. T. Matsushima, Y. Kinoshita, H. Murata. *Appl. Phys. Lett.* **91**, 253504 (2007).
137. J.-H. Li, J. Huang, Y. Yang. *Appl. Phys. Lett.* **90**, 173505 (2007).
138. M. Kröger, S. Hamwi, J. Meyer, T. Riedl, W. Kowalsky, A. Kahn. *Appl. Phys. Lett.* **95**, 123301 (2009).
139. C. Tao, S. Ruan, X. Zhang, G. Xie, L. Shen, X. Kong, W. Dong, C. Liu, W. Chen. *Appl. Phys. Lett.* **93**, 193307 (2008).
140. C. Tao, S. P. Ruan, G. H. Xie, X. Z. Kong, L. Shen, F. X. Meng, C. X. Liu, X. D. Zhang, W. Dong, W. Y. Chen. *Appl. Phys. Lett.* **94**, 043311 (2009).
141. D. Y. Kim, J. Subbiah, G. Sarasqueta, F. So, H. J. Ding, Irfan, Y. L. Gao. *Appl. Phys. Lett.* **95**, 093304 (2009).
142. I. Hancox, K. V. Chauhan, P. Sullivan, R. A. Hatton, A. Moshar, C. P. A. Mulcahy, T. S. Jones. *Energy Environ. Sci.* **3**, 107 (2010).
143. J. Meyer, A. Shu, M. Kroger, A. Kahn. *Appl. Phys. Lett.* **96**, 133308 (2010).
144. C. H. Cheung, W. J. Song, S. K. So. *Org. Electron.* **11**, 89 (2010).
145. J. Gao, J. M. Luther, O. E. Semonin, R. J. Ellingson, A. J. Nozik, M. C. Beard. *Nano Lett.* **11**, 1002 (2011).
146. J. Subbiah, D. Y. Kim, M. Hartel, F. So. *Appl. Phys. Lett.* **96**, 063303 (2010).
147. Irfan, H. Ding, Y. Gao, D. Y. Kim, J. Subbiah, F. So. *Appl. Phys. Lett.* **96**, 073304 (2010).
148. G. P. Xu, S. L. Ji, C. H. Miao, G. D. Liu, C. H. Ye. *J. Mater. Chem.* **22**, 4890 (2012).
149. Z. Tachan, M. Shalom, I. Hod, S. Ruehle, S. Tirosh, A. Zaban. *J. Phys. Chem. C* **115**, 6162 (2011).
150. Y. R. Smith, V. Subramanian. *J. Phys. Chem. C* **115**, 8376 (2011).

